Dynamics of Carbon Monoxide Binding with Cytochromes P-450†

Catherine Tétreau,‡ Carmelo Di Primo,§ Reinhard Lange,|| Hervé Tourbez,‡ and Daniel Lavalette*,‡

Institut Curie, INSERM U350, Bat. 112, Centre Universitaire, 91405 Orsay, France, Institut de Biologie Physico-chimique, INSERM-INRA U310, 13, rue Pierre et Marie Curie, 75005 Paris, France, and INSERM U128, route de Mende, BP5051, 34033 Montpellier, France

Received March 18, 1997; Revised Manuscript Received May 29, 1997⊗

ABSTRACT: The dynamics of CO rebinding with cytochromes P-450$_{cam}$, P-450$_{scc}$, and P-450$_{LM2}$ after laser flash photolysis have been investigated from 293 to 77 K, and the distribution functions of the rate parameters $P(k)$ and of the activation enthalpy $P(H)$ were determined using the maximum entropy method. In a fluid solvent, geminate rebinding is nonexponential, presumably because of a spectral shift induced by protein relaxation on the same time scale. Substrate binding increases the yield of the bimolecular process and decreases the bimolecular rate by 1 or 2 orders of magnitude. The amplitude of these effects seems to correlate with substrate specificity. In a rigid environment at low temperature, cytochromes P-450 exhibit a bimodal distribution of activation enthalpy; $P(H)$ consists of two distinct bands which are in a thermal equilibrium even at 77 K. The results lead to a scheme in which a common structural perturbation splits the conformational substates of cytochromes P-450 into pairs of "doublet" substates with different dynamic properties. The hierarchy of conformational substates of cytochromes P-450 thus contrasts with that of oxygen-binding hemoproteins such as myoglobin.

Most of present-day concepts on protein dynamics have come from numerous studies devoted to hemoglobin and myoglobin. At least three reasons made these oxygen transport and storage hemoproteins ideal models for investigating the relationship between protein structure, dynamics, and function: (*i*) the three-dimensional X-ray structures were determined early; (*ii*) they bind simple ligands such as O_2, CO, NO, or cyanides and display good spectroscopic markers which are characteristic of the ligation state of their reactive prosthetic group, the heme; (*iii*) the heme−ligand bond is photolabile. This property opened the way to time-resolved investigation using flash photolysis. In particular flash photolysis experiments performed in a rigid environment at low temperatures have contributed greatly to our understanding of the dynamic behavior of proteins. The picture that has emerged (Austin et al., 1975) can be summarized as follows: a protein can assume a variety of energetically similar conformational substates (CS), which slightly differ in their activation enthalpy for ligand binding. Protein molecules in different substates rebind at slightly different rates. The thermodynamics and the kinetics of a protein ensemble are therefore best described by probability distributions of the activation enthalpy H and of the reaction rate parameter k, $P(H)$ and $P(k)$, respectively. The rate distribution shows itself as nonexponential geminate kinetics when fluctuations between substates are hindered, as is the case in a rigid environment (e.g. below the glass transition temperature of the solvent). On the contrary, in a fluid environment (e.g. at room temperature), ligand rebinding appears exponential because rapid equilibrium fluctuations between substates cause $P(k)$ to collapse into a unique average value.

These features have been shown later to apply not only to hemoproteins but also to the non-heme oxygen carrier hemerythrin (Lavalette et al., 1991) and to the electron carrier copper protein azurin (Ehrenstein & Nienhaus, 1992). Various methods have been successively used to recover the enthalpy distributions $P(H)$ from the observed kinetics (Austin et al., 1975; Lavalette et al., 1991; Steinbach et al., 1991). The correlation between $P(H)$, $P(k)$, and thermodynamic as well as kinetic parameters at room temperature have been discussed in detail (Ansari et al., 1986; Lavalette et al., 1991).

Two additional features have recently been added to the general framework derived from the study of carboxymyoglobin: (*i*) above about 180 K, the kinetics are further complicated by a relaxation process which affects the whole protein and which occurs on the time scale of the rebinding reaction (Steinbach et al., 1991; Nienhaus et al., 1992; Lim et al., 1993; Ansari et al., 1994). (*ii*) CS constitute a hierarchy (Ansari et al., 1985; Ansari et al., 1987). The higher members, CS^0, are based on a few conformers which bind CO with different geometries. CS^0 are well characterized by infrared CO stretch bands. Nonexponential CO rebinding kinetics, monitored by IR spectroscopy, showed that each CS^0 is composed of a collection of conformational substates, CS^1 (Ansari et al., 1987; Berendzen & Braunstein, 1990; Mourant et al., 1993; Johnson et al., 1996).

Compared with this wealth of information on the dynamics of myoglobin, little is known about other photoreactive proteins such as cytochromes P-450 which constitute another class of hemoproteins with important and complex enzymatic functions. Even if these monooxygenases share a common active site consisting of a thiolate-coordinated iron proto-

† This work was supported, in parts, by a "Contrat cooperatif" from the Institut Curie.

* Author to whom correspondence should be addressed. Phone: 33-1-69 86 31 81. Fax: 33-1-69 86 31 56. E-mail: Daniel.Lavalette@curie.u-psud.fr.

‡ INSERM U350.

§ INSERM-INRA U310.

|| INSERM U128.

⊗ Abstract published in *Advance ACS Abstracts,* August 1, 1997.

[1] Abbreviations: Mb, myoglobin; CS, conformational substates; Hb, hemoglobin; MEM, maximum entropy method.

S0006-2960(97)00619-3 CCC: $14.00 © 1997 American Chemical Society

porphyrin IX, they display a great diversity of biological functions such as activation of procarcinogens, detoxification of xenobiotics, and steroid biosynthesis. They also greatly differ in their substrate specificity. Thus, this family offers a unique opportunity to examine the regulatory role of the protein matrix and to investigate the relationship between protein/substrate/ligand dynamics and function.

Because additional complexity could be expected from the presence of the substrate in the heme pocket, we have performed kinetic investigations with three different cytochromes P-450 in their substrate-free form as well as with their CO−substrate ternary complexes. The cytochromes selected for this work were P-450$_{cam}$, P-450$_{scc}$, and P-450$_{LM2}$; while the two former are representative of cytochromes with narrow specificity, the latter has a broad specificity. Bacterial cytochrome P-450$_{cam}$ is a soluble protein from *Pseudomona putida* which catalyzes the stereospecific hydroxylation of camphor at the 5-exo position. P-450$_{LM2}$ is a microsomal cytochrome which is induced in rabbit liver by phenobarbital. P-450$_{scc}$ is a mitochondrial cytochrome of the adrenal cortex which is responsible for the cleavage of the sidechain of cholesterol to produce pregnenolone.

The goal of this work was to examine to what extent the features of cytochromes P-450 match the models derived from Mb. For this purpose the kinetics of CO rebinding after laser flash photolysis have been investigated from 293 to 77 K and the distribution functions $P(k)$ and $P(H)$ were determined using the maximum entropy method. It turns out that cytochromes P-450 share a number of common properties with Mb but that the hierarchy of CS is significantly different in these two proteins.

MATERIALS AND METHODS

Materials

Cytochrome P-450$_{scc}$ (CYP11A1) was isolated from the inner mitochondrial membrane of bovine adrenal cortex as described (Suhara et al., 1978; Lange et al., 1988). Removal of endogenous substrate (cholesterol) was carried out as described (Larroque & Van Lier, 1986).

Cytochrome P-450$_{LM2}$ (CYP2B4) was isolated from liver microsomes of phenobarbital-treated New Zealand white rabbits (Imai et al., 1980); benzphetamine (from Sigma) was used as a substrate.

Recombinant cytochrome P-450$_{cam}$ (CYP101) was generated and purified as previously described (Unger et al., 1986). The substrate-free form of the protein was obtained by passage of a pure concentrated sample through a Sephadex G-25 column.

The required amount of cytochrome P-450 was diluted with glycerol, buffer, and water to reach final working concentrations of 10−15 μM in protein, 50 mM in phosphate or Tris buffer, and 70% (w/w) glycerol. The solubility of CO in 70% glycerol was taken as 0.5 mM. The ferrous CO complexes were prepared by passing a stream of CO above the protein solution submitted to gentle stirring and adding a few microliters of a concentrated deaerated dithionite solution. The CO binding was controlled by following the absorption change of the solution. The reduction was complete after a few minutes for P-450$_{LM2}$ and P-450$_{cam}$, and after an incubation time of about 30 min for P-450$_{scc}$.

Methods

1. Data Collection. Carbonylated cytochrome P-450 solutions in gas tight square cuvettes were inserted in a liquid nitrogen cryostat (Oxford Instruments DN704). The sample was cooled slowly below T_g in about 20 min. Systematic records were performed by cooling the sample in steps of 10 K at a rate of 1 K/min and allowing 15 min equilibration once the desired temperature was attained. This procedure was slow enough to achieve thermal homogeneity of the sample. However, the total cooling time between successive temperatures remained short compared to glass relaxation (Ansari et al., 1987). Thus, relaxation processes of the glassy matrix do not interfere with the kinetic measurements.

Photodissociation was achieved by the 10 ns pulse of the second harmonic (532 nm) of a Q-switched Nd-YAG laser (Quantel, France). The absorption was monitored at a right angle from the excitation direction using a grating monochromator and a low gain−high current photomultiplier. The signal to noise ratio was optimized by adjusting the response time constant. Depending on the scan rate, either a 75 W xenon arc (pulsed or cw) or a cw 100 W quartz−iodine lamp provided the analyzing beam. The signal from the photomultiplier was digitized by a Lecroy 9450 digital oscilloscope. A reference channel for the analyzing light intensity was provided by a homemade electronic back-off unit. For subsequent processing the data were transferred to an Apple Macintosh Quadra 650 computer via an IEEE-488 interface.

Since carbonylated hemoproteins are known to be highly photosensitive, the monitoring beam was attenuated by inserting neutral filters on the light path, in order to achieve an optimal compromise between the background photolysis and the signal to noise ratio. Transient absorption changes, monitored at the peak of the Soret band (445−450 nm), could be followed over 2 decades in amplitude and 6−7 decades in time.

2. Data Processing. A software has been developed to prepare the data for the treatment by MEM. Transmittance information is first transformed into absorbance changes using the calibrated reference channel of the back-off unit. Noise statistics were also automatically performed for each data point, taking into account the instantaneous absorbance.

Since low-temperature kinetics extend over several orders of magnitude in time, the use of a logarithmic clock is recommended (Austin et al., 1976). To this end we process the linear time base with our software. Data from several runs at different scan rates are first pieced together after performing an appropriate renormalization based on a numerical integration of areas of two successive and temporally overlapping scans. This procedure minimizes the difficulties brought about by noisy signals. Noise estimates are also renormalized accordingly. We have devised a "logarithmic smoothing" subroutine to convert the data to a logarithmic time base, as required by MEM (see below), while taking advantage of the large number of data points to improve the signal to noise ratio. We arbitrarily define a set of logarithmically spaced times

$$t_n = t_0 \exp(\lambda n) \tag{1}$$

where λ^{-1} is the number of points per log unit. It is easy to show (unpublished results) that the integral average of $\exp(-kt)$ between t_{n-1} and t_{n+1} is virtually equal to

$$\langle e^{-kt} \rangle = e^{-kt_n} \frac{\sinh(\lambda k t_n)}{\lambda k t_n} \quad (2)$$

The limit of the second factor is unity within a few thousands if $\lambda^{-1} \leq 10$. In practice, the kinetics are averaged by integration between the data points closest to t_{n-1} and t_{n+1}, and the result is assigned to the intermediate time $t_n = (t_{n+1}t_{n-1})^{1/2}$. Simulations showed that with 10−20 points per decade no detectable error occurred. As long as the kinetics consist of a sum of exponentials, the procedure will yield a limited number of points of great accuracy which reproduce the whole time course without distortion.

3. Distribution of Rate Parameters Using the Maximum Entropy Method. At low temperature the kinetics, expressed by the survival fraction $N(t)$ of unrecombined molecules, are given by the weighted infinite sum of exponentials (Austin et al., 1975):

$$N(t) = \int_0^\infty P(k) e^{-kt} \, dk \quad (3)$$

In recent years, the problem of inverting the Laplace transform (3) to get $P(k)$ from the observed kinetics $N(t)$ has been solved by using the maximum entropy method (MEM) for fluorescence decay curves (Livesey et al., 1987a; Livesey & Brochon, 1987b) as well as for low-temperature kinetics in flash photolysis (Lavalette et al., 1991; Steinbach et al., 1991,1992; Johnson et al., 1996). MEM gives the most probable distribution of exponentials $P(k)$ fitting $N(t)$ *within the stated accuracy of the experimental data*. In this work, we used a suitably modified version of the program previously applied to the analysis of fluorescence lifetimes and based on the Cambridge algorithm and on the Memsys5 package (Maximum Entropy Data Consultants Ltd, Cambridge). $P(k)$ was developed on a discrete basis of logarithmically spaced k_i values. The amplitudes of the k_i's were iteratively adjusted subject to the dual constraints of minimizing a χ^2 statistic

$$\chi^2 = \left\langle \frac{(N_{calc} - N_{exp})^2}{\sigma^2} \right\rangle \quad (4)$$

(where σ^2 is the variance of the individual data points), and simultaneously maximizing S, the entropy of the $P(k_i)$ probability set

$$S = -\sum_i P(k_i) - m_i - \log[P(k_i)/m_i] \quad (5)$$

where m_i is an arbitrary initial amplitude.

The computation was carried out on a Silicon Graphics Iris Power Series 4D320 workstation. The starting distribution of m_i was taken as equiprobable with an amplitude equal to 10^{-3} times the initial amplitude of the kinetic scan. The computation was stopped when the value $\chi^2 = 1$ was reached, i.e. when the temporal fit was, on average, as good as that permitted by the accuracy of the data points. Noise estimation was therefore very critical, especially to distinguish between discrete and continuous distributions. We consistently regarded as real structure only those features which clearly persisted even after arbitrarily doubling the σ^2 values.

It has been shown that MEM is optimized when the basis set of k_i is logarithmically spaced (Livesey & Brochon, 1987b). In low-temperature flash photolysis one expects $P(k)$ to be broad and continuous. Computations with simulated kinetics covering many time decades have convinced us that the use of a logarithmic time scale is also a necessary requirement for MEM to give consistent results. With a linear time scale, the number of data points sampled by the log k basis increases exponentially as time proceeds. Thus, low "frequencies" greatly outweigh the statistics, and temporal fits at short times are poor. Clearly, time and "frequency" domains must be treated on an equal footing for the Laplace inversion to work properly. In other words, if we use a log k space, we must transform eq 3 into

$$N(t) = \int_0^\infty P(\log k) \exp(-e^{\log k + \log t}) \, d(\log k) \quad (6)$$

suggesting that $N(t)$ is actually $N(\log t)$.

The results of many such simulations indicated that with 10−20 time data points per decade, the initial $P(k)$ could be recovered within any desired accuracy (depending on the amount of added noise) using 100 channels of equidistant log k values over the range $1-10^{10}$ s^{-1}. The use of a logarithmic time scale is therefore not only a necessity for optimizing signal to noise ratio; it is also a computational requirement.

4. Computing the Enthalpy distribution P(H). The basic assumption is that below the solvent's glass transition temperature, T_g, all kinetics should be derived from one unique probability distribution of activation enthalpy (Austin et al., 1975).

For simplicity, at all temperatures $T < T_g$ we shall write $P(H) = P(H,T_g)$. When necessary, $P(H)_T$ will denote the experimental distribution $P(H)$ obtained from kinetic data recorded at temperature T. In the absence of experimental errors, all $P(H)_T$ should be equal to $P(H)$. Because the rate parameter k and the activation enthalpy H are connected by

$$H = RT \ln A - RT \ln k \quad (7)$$

the correspondence between rate and enthalpy probability distributions may be written as

$$P(H)_T \, dH_T = P(-RT \ln k) \, d(-RT \ln k) \quad (8)$$

$$P(H)_T \, dH_T = P(h) \, dh$$

in which we define the variable $h = RT \ln k$ which has the dimensions of an enthalpy.

Since MEM directly outputs $P(\ln k)$, a simple change of coordinates followed by renormalization yields the $P(H)$ profile. However, in order to determine its position on the H scale, the pre-exponential factor A must be known. If we were dealing with narrow lines, an Arrhenius plot would be sufficiently accurate. Unfortunately, with broad and continuous distributions, the data are generally not good enough to warrant a perfect superposition of the $P(h)$ profiles at different temperatures. In order to average out small fluctuations in the shape of $P(h)$ bands, we compute the barycentre $B(h)$ of the distribution:

$$B(h) = \int h P(h) \, dh \quad (9)$$

By means of eq 7 one easily derives

$$B(h) = RT \ln A - B(H) \quad (10)$$

Upon increasing the temperature, $P(h)$ uniformly moves along the h axis with a rate equal to $R \ln A$, keeping the shape of $P(H)$ constant. The pre-exponential factor and the barycentre of $P(H)$ are obtained from the linear plot of a series of $P(h)$ at different temperatures.

All known procedures to extract $P(H)$ from kinetic data are based on the assumption of a single value for the pre-exponential factor A. The assumption has always yielded consistent results (Austin et al., 1975; Lavalette et al., 1991; Ehrenstein & Nienhaus, 1992). Recently, two-dimensional MEM has been tentatively applied to test a more general model in which both H and A were distributed (Steinbach, 1996). The conclusion was that, whereas in principle feasible, the simultaneous recovery of $P(A)$ and $P(H)$ would require an experimental accuracy which is far beyond the possibilities of current instrumentation.

RESULTS

1. Fluid Environment at Room Temperature. At 293K in a fluid solvent, the rate of conformational fluctuations is much faster than that of rebinding. The kinetics are therefore expected to consist of discrete exponentials and $P(k)$ of narrow, noise-limited, lines. Under these conditions, carbonylated cytochromes P-450 follow the same elementary kinetic scheme (Scheme 1) as other proteins which bind a photolabile ligand.

A denotes the state in which CO is bound to the heme. In state B the heme−CO bond has been photodissociated but the ligand remains within the protein. In S the ligand has left the protein and may exchange freely with other ligand molecules in the solvent.

Scheme 1

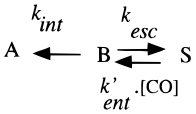

The kinetics of CO rebinding with the three different cytochromes in their substrate-free (m^r_{co}) and substrate-bound (m^{rs}_{co}) forms at 293 K are displayed in Figure 1. The corresponding normalized distributions of the rate parameters obtained by MEM analysis are shown in Figure 2. Numerical values are listed in Table 1.

Two well-characterized rebinding processes can be distinguished. The initial, faster phase observed in the time range 10−500 ns was independent of CO concentration. It corresponds to the geminate process, i.e. to CO molecules which recombine without leaving the protein. For the three-state model (Scheme 1) the geminate rate is

$$k_{gem} = k_{int} + k_{esc} \qquad (11)$$

The rate of the subsequent, slower phase, observed in the time range 100 μs to 100 ms, varied linearly with the CO concentration. This characterizes a bimolecular rebinding process after diffusion of CO out into the solvent with a rate equal to k'_{on}. Geminate and bimolecular rebinding processes appear as well-separated groups of bands located respectively in the high (6−8 log k units) and low (2−4 log k units) rate region of $P(k)$. The proportion of molecules rebinding *via* the bimolecular process is given by

$$N_{esc} = k_{esc}/k_{gem} \qquad (12)$$

N_{esc} is estimated using the band integrals (Figure 2).

No geminate phase was observed with substrate-bound P-450$_{cam}$ and P-450$_{scc}$ ($N_{esc} \approx 1$). Instead, the rebinding kinetics showed a small but significant initial absorbance increase with a rate independent of the CO concentration. In addition, the rate of this process was observed to vary with the solvent's viscosity approximately as $\eta^{-0.6}$ in the range 1−150 cP. The results (not shown) are not quantitatively very accurate, because the signal has to be subtracted from the overall rebinding kinetics. But the viscosity dependence is not questionable, and contrasts with the constant rate of the bimolecular phase in the same viscosity range. We tentatively attribute this signal to a spectral shift induced by a slow relaxation of the protein toward the equilibrated ligand-free conformation (Discussion, section 1.3).

1.1. Cytochrome P-450$_{cam}$. Bimolecular rebinding of P-450$_{cam}$ in its substrate-free form was distinctly biphasic. However the value of the slower rate closely matched that of camphor-bound P-450$_{cam}$, and its amplitude was found to depend on the sample under investigation. Obviously this component (also reported by others (Tian et al., 1995)) is due to residual traces of substrate which cannot be completely removed. The removal of camphor by gel filtration was controlled by measuring the absorption of the Fe^{III} form which peaks at 396 and 417 nm for the camphor-bound and the camphor-free protein, respectively. Even though a small contamination by the camphor-bound form could hardly be detected by absorption, one must keep in mind that its contribution to the total bimolecular signal would be considerably amplified because the yield of the bimolecular process is increased by a factor of 10−20 upon camphor fixation.

While two geminate bands are also observed, the slowest one contributes only a small amount to the total geminate decay. Substrate binding with P-450$_{cam}$ has profound consequences. Indeed, whereas rebinding is mostly geminate in the substrate-free form ($N_{esc} \approx 0.12$), no geminate rebinding was detected for the substrate-bound form. Moreover, the bimolecular association rate constant is reduced by more than 2 orders of magnitude by the presence of camphor (Figure 2). Tian et al. (1995) have reported biphasic bimolecular and geminate rebinding with P-450$_{cam}$ in 75% glycerol. While they suggested that P-450$_{cam}$ could present two different conformations which do not exchange on the time scale of CO recombination, their time resolution (10−20 ns), although comparable to ours, is certainly not sufficient to allow an accurate determination of the rate of the major fast geminate phase (Discussion, section 2.1).

1.2. Cytochrome P-450$_{scc}$. Noticeable changes in both the yield of CO escape and the rebinding kinetics are induced by cholesterol binding with P-450$_{scc}$. The yield of CO escape increases from 0.68 to 1.00, while the CO bimolecular association rate decreases by 1 order of magnitude (Table 1). The second-order rate constant of P-450$_{scc}$ m^{rs}_{co} agrees well with all previous determinations (Tuckey & Kamin, 1983; Mitani et al., 1985; Kashem et al., 1987; Lange et al., 1994); for the substrate-free form, our value agrees with that determined by Mitani *et al*. (1985), but differs by 1 order of magnitude from those obtained by Tuckey & Kamin (1983) and Kashem et al. (1987) using stopped-flow spectrophotometry. The origin of this difference is not understood. Some unresolved structure may be hidden below the wide $P(\log k)$ bands of P-450$_{scc}$ m^r_{co} (Figure 2). Recent studies

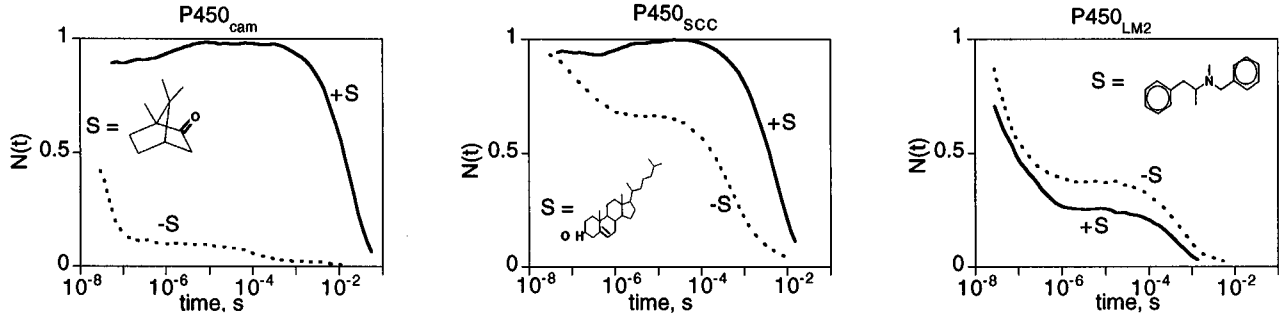

FIGURE 1: Kinetics of CO rebinding with the substrate-free (dotted lines) and substrate-bound (full lines) forms of cytochromes P-450, measured at the peak of the Soret band (445−450 nm) at 293 K in 70% glycerol with [CO] = 0.5 mM. $N(t)$ represents the fraction of the photodissociated molecules that have not yet rebound at time t. The average error of data points is about 1%.

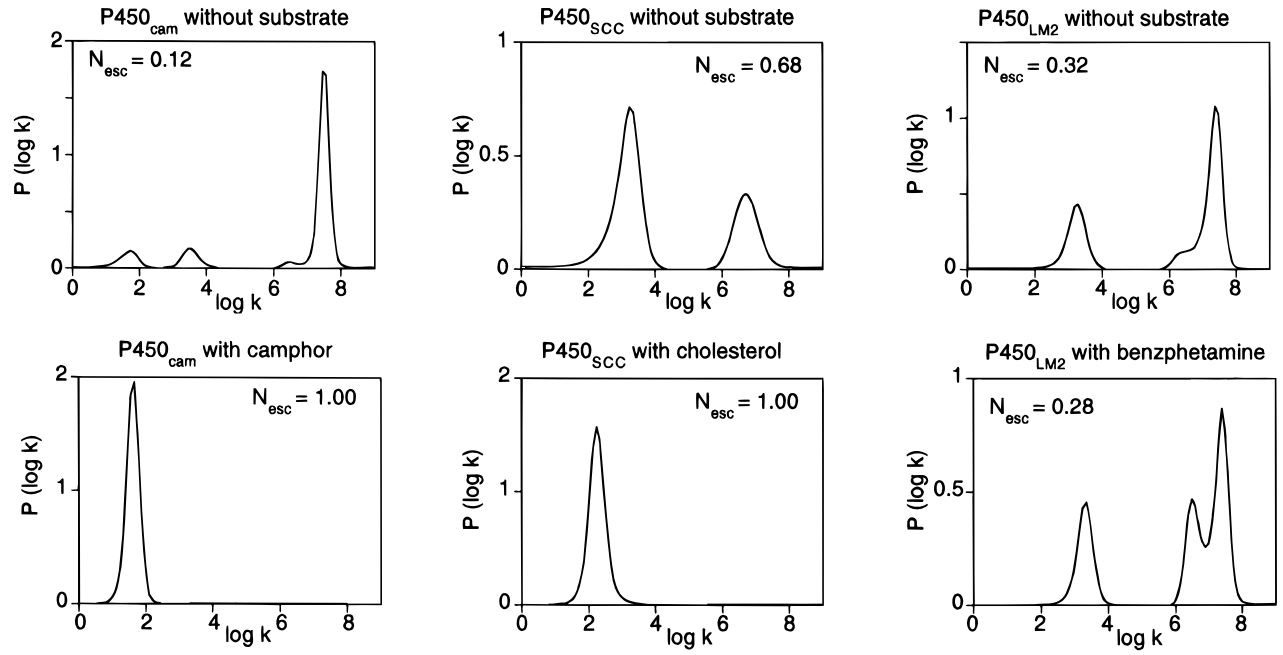

FIGURE 2: Normalized $P(k)$ distributions corresponding to Figure 1. The ligand escape yield (N_{esc}) was calculated from the area of the bimolecular MEM bands (the total area being equal to unity). This assumes that no process faster than $1 \times 10^8 - 1 \times 10^9$ s^{-1} takes place. Since such a process would escape detection, N_{esc} is strictly a higher limit to the true escape yield. For substrate-free P-450$_{cam}$, the spurious leftmost band was not included in the calculation of N_{esc} (see text). For substrate-bound P-450$_{cam}$ and P-450$_{scc}$, MEM analysis was restricted to the decaying part of the kinetics.

Table 1: MEM Analysis of the Kinetics of CO Rebinding with Cytochromes P-450 Measured at 293 K in 70% Glycerol[a]

molecule	$k_{gem,fast}$ (10^7 s^{-1})	%	$k_{gem,slow}$ (10^7 s^{-1})	%	$k'_{on,fast}$ (10^7 M^{-1} s^{-1})	%	$k'_{on,slow}$ (10^7 M^{-1} s^{-1})	%
P-450$_{cam}$ m$^r_{co}$	2.8	72	0.3	4	0.7	12	0.01	12
P-450$_{cam}$ m$^{rs}_{co}$		0		0	0.01	100		0
P-450$_{LM2}$ m$^r_{co}$	2.3	54	0.3	13	0.3	32		0
P-450$_{LM2}$ m$^{rs}_{co}$	2.4	45	0.3	27	0.4	28		0
P-450$_{scc}$ m$^r_{co}$	0.5	33		0	0.3	67		0
P-450$_{scc}$ m$^{rs}_{co}$		0		0	0.03	100		0

[a] The rate parameters correspond to the values measured at the peak of the distributions. The relative contributions were calculated from the relative band areas.

of the spin-state equilibrium (Lange et al., 1992a,b) and of the resonance Raman spectra (Hildebrandt et al., 1994) of the ferric forms of P-450$_{scc}$ suggest that, in a pure aqueous buffer at 295 K, the protein exists as two different species in a 3/1 ratio. In order to account for the widths of the P(log k) bands (Figure 2), one has to assume that bimolecular CO rebinding rates with either conformations differ in the absence of substrate (wide band) but practically collapse in the presence of substrate (narrow band). In view of the experimental data we can neither prove nor disprove this possibility.

P-450$_{scc}$ m$^r_{co}$ exhibits only one geminate band, but its width is significantly broader than the noise-limited bandwidth (about 0.6 log units), suggesting once more the possibility of a hidden, nonresolved, structure.

1.3. Cytochrome P-450$_{LM2}$. The yield of CO escape from P-450$_{LM2}$ and the rate constants are practically unaffected by substrate fixation (Table 1). The only significant change brought about by substrate fixation is an increase of the relative amplitude of the slow geminate phase compared to the faster one. The values of the second-order association rate parameters (Table 1) are consistent with previous

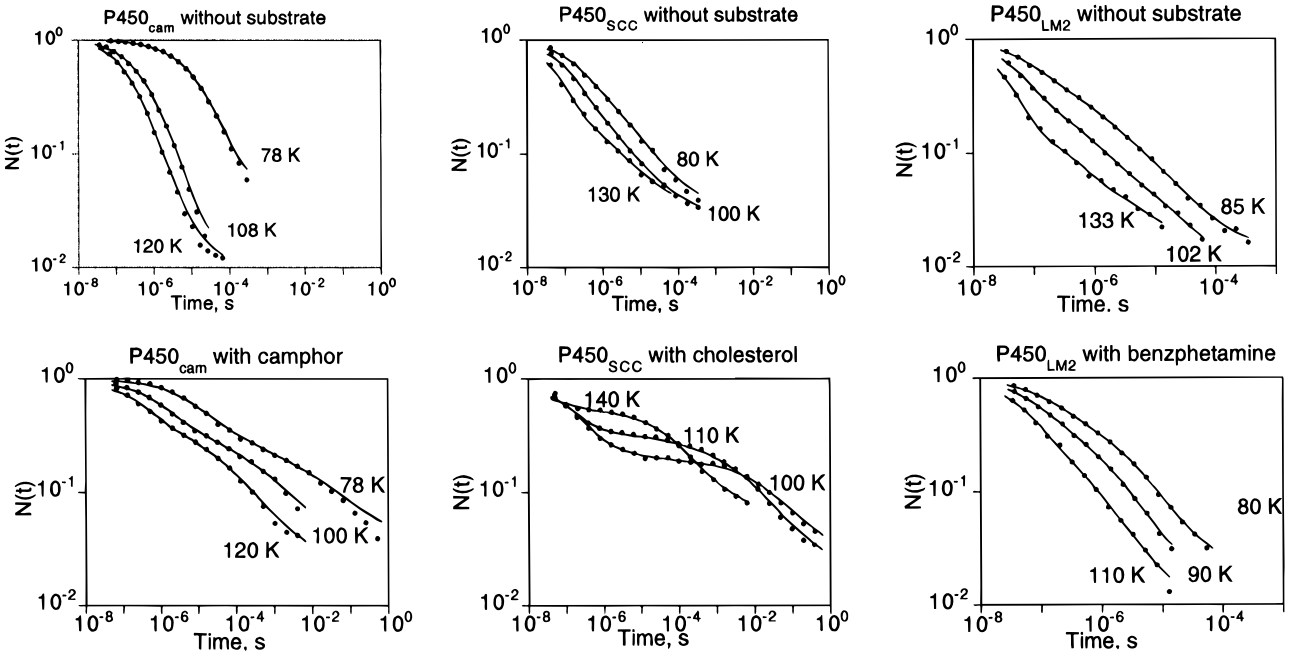

FIGURE 3: CO geminate rebinding kinetics below the freezing point of the solvent (T_g = 165 K) in 70% glycerol. Substrate-free (top) and substrate-bound (bottom) forms of cytochromes P-450. Symbols represent data points. Solid lines are MEM fits to the data. The average error of data points is about 1%.

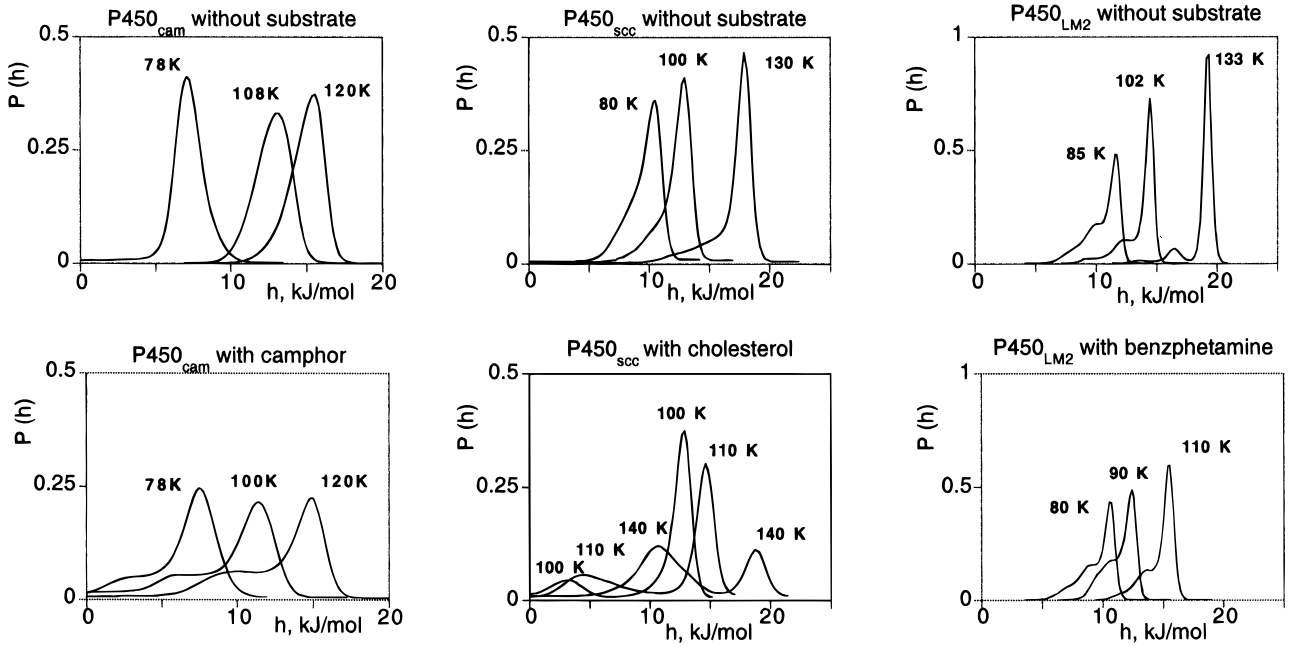

FIGURE 4: $P(h) = P(RT \ln k)$ (see Materials and Methods) calculated by MEM from the kinetics of Figure 3. Substrate-free (top) and substrate-bound (bottom) forms of cytochromes P-450. Note that if the enthalpy distributions were invariant below T_g, the shape of $P(h,T)$ should also remain invariant (by eq 7), a situation which is observed only for P-450$_{cam}$ m$^r_{co}$.

determinations (Gray, 1982; Lange et al., 1994). Although kinetic heterogeneity has been reported and attributed to heterogeneity of the proteins (Oertle et al., 1985) or of the membrane environment (Lange et al., 1994), we found no evidence of kinetic heterogeneity in bimolecular rebinding of CO with P-450$_{LM2}$.

In contrast, the structure of the geminate band of P-450$_{LM2}$ m$^r_{co}$ and m$^{rs}_{co}$ indicates the presence of two overlapping bands.

2. Rigid Environment and Low Temperatures. The amplitude of the bimolecular process progressively decreased upon decreasing of the temperature and vanished at about 200 K. Below 200 K the high viscosity of the medium prevented CO escape from the protein, and only the geminate process from within the protein subsisted ($k_{gem} = k_{int}$). Unless otherwise stated, all data refer to the temperature range 77−145 K, which is below the solvent's glass transition temperature ($T_g \approx 165$ K). At these temperatures the protein conformational fluctuations are suppressed. Nonexponential kinetics were observed for all cytochromes under these conditions (Figure 3). The rate distributions are given in Figure 4 as $P(h,T) = P(RT \ln k,T)$ because this representation allows one to better visualize the shape of the enthalpy distribution (see Materials and Methods). We describe the simpler case of P-450$_{cam}$ m$^r_{co}$ first and then proceed to the other forms of P-450.

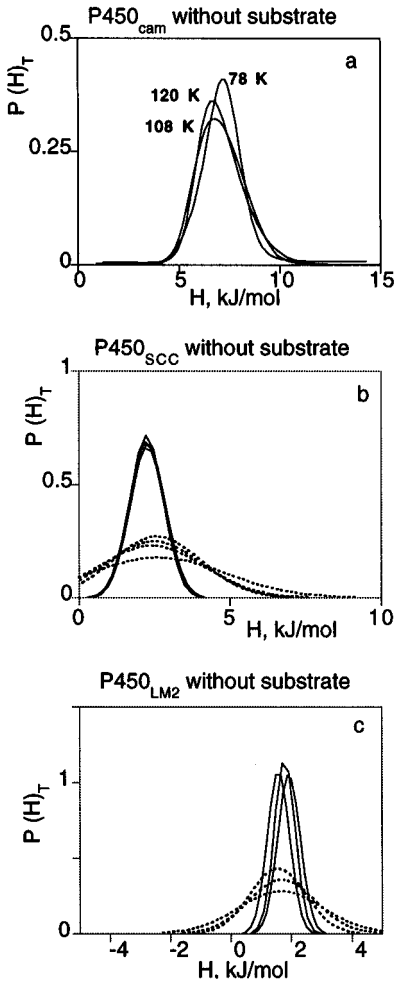

FIGURE 5: Determining the normalized enthalpy distributions $P(H)$ for carbon monoxide rebinding with cytochromes P-450 in 70% glycerol below the glass transition temperature: (a) substrate-free form of cytochrome P-450$_{cam}$; (b) substrate-free form of cytochrome P-450$_{scc}$; (c) substrate-free form of P-450$_{LM2}$. $P(H)_T$ was fitted using one (a) or two (b, c) gaussians. The subdistributions have been independently normalized. Information about the relative amplitude of the subpopulations is lost, but the invariance of $P(H)_T$ below T_g can be checked. Full and dotted lines correspond to the enthalpy distributions of the "fast" and "slow" reacting sets of substates, respectively.

2.1. P-450$_{cam}$ m$^r_{co}$. The kinetics of CO rebinding with P-450$_{cam}$ m$^r_{co}$ (Figure 3) were smooth and continuously slowed down upon decreasing the temperature. $P(h)$ remains unimodal, but the band shifts toward lower ln k values upon decreasing of the temperature (Figure 4). The half bandwidth of this unique $P(h)$ band is much larger than the noise-limited width of 0.8 kJ/mol, indicating that the activation enthalpy is distributed. The pre-exponential factor (Table 2) was obtained from the slope of the linear plot of the barycentre of the $P(h)$ distributions as a function of RT as described under Materials and Methods (eq 10). Enthalpy distributions $P(H)_T$ calculated at 78, 108, and 120 K are identical within errors (Figure 5a). This confirms the absence of protein fluctuations in the rigid environment as well as the temperature invariance of the enthalpy distribution below the glass transition temperature. However, $P(k)$ changes when the temperature is further lowered because the Arrhenius relation connects each rate with $P(H,T_g)$. The enthalpy distribution $P(H)$ of P-450$_{cam}$ m$^r_{co}$ is rather symmetrical (Figure 5a) and can be reasonably well described by a gaussian. Remarkably the MEM distribution is in very good agreement with an early report by Eisenstein *et al.* (1977) who approximated the rebinding curves by an analytical model which was subsequently Laplace-inverted.

2.2. Other Forms of P-450. In contrast with P-450$_{cam}$ (m$^r_{co}$), all other forms of cytochromes P-450 presented complex kinetics with either undulations or even two distinct components (Figure 3). $P(h,T)$ then consists of two or three bands with different amount of overlap (Figure 4).

But the most striking feature of cytochromes P-450 kinetics is the change of shape of $P(h)$ with temperature (Figure 4). These features could be constantly reproduced with different samples and different cooling cycles. Thus, $P(h)$ cannot be attributed to a unique multimodal $P(H)$ distribution but rather to a superposition of independent enthalpy subdistributions. This surprising feature of the cytochrome dynamics complicates the computation of the enthalpy distribution(s). To quantify the contribution of the subdistributions we must assume a specific band shape. By analogy with P-450$_{cam}$ (m$^r_{co}$) the composite $P(h)$ were fitted with the sum of two or three gaussians. The treatment outlined in the case of one single band was then applied to each individual gaussian in order to determine its associated pre-exponential factor and enthalpy subdistribution.

As an example, Figure 5b shows the subdistributions $P_{fast}(H)_T$ and $P_{slow}(H)_T$ of P-450$_{scc}$ m$^r_{co}$ after independent normalization at four different temperatures. As expected for nonfluctuating subpopulations of CS, each is reasonably independent of temperature. At the present level of accuracy the gaussian band shape therefore appears to be a sufficient approximation. P-450$_{LM2}$ m$^r_{co}$ and P-450$_{LM2}$ m$^{rs}_{co}$ presented an additional difficulty. The MEM spectra (Figure 4) are relatively narrow and exhibit two maxima and a shoulder at each temperature. A fit with three gaussians yielded a moderately well defined major band but showed considerable scatter of the minor bands; even physically unacceptable negative enthalpy values were observed. The results obtained using only two gaussians were more stable (Figure 5c). From here on we consistently adopted this description, keeping in mind that a third minor band could also provide a weak contribution to the rate and enthalpy distributions. The final normalized $P(H)$ values of all six systems investigated in this work are given in Figure 6 in which the average distributions were calculated by merging the $P(H)_T$ obtained at different temperatures between 78 and 160 K. The parameters characterizing enthalpy subdistributions of the various cytochromes are listed in Table 2.

The complete enthalpy distribution of the protein must now be described by

$$P(H,T) = \alpha_{fast}(T)P_{fast}(H) + \alpha_{slow}(T)P_{slow}(H) \quad (13)$$

in which the α_i are the temperature dependent relative contributions of the two bands. Assuming equal extinction coefficients for the Fe(II) and Fe(II)−CO states, $\alpha_{fast}(T)/\alpha_{slow}(T)$ is also equal to the ratio of the protein subpopulations. This assumption is supported by the fact that the sample transmission does not change appreciably over the whole range of temperatures. Even though $T < T_g$, Figure 7 shows that $\alpha_{fast}(T)/\alpha_{slow}(T) = \exp(-\Delta G/RT)$. The parameters of the equilibrium between the subpopulations are given in Table 3.

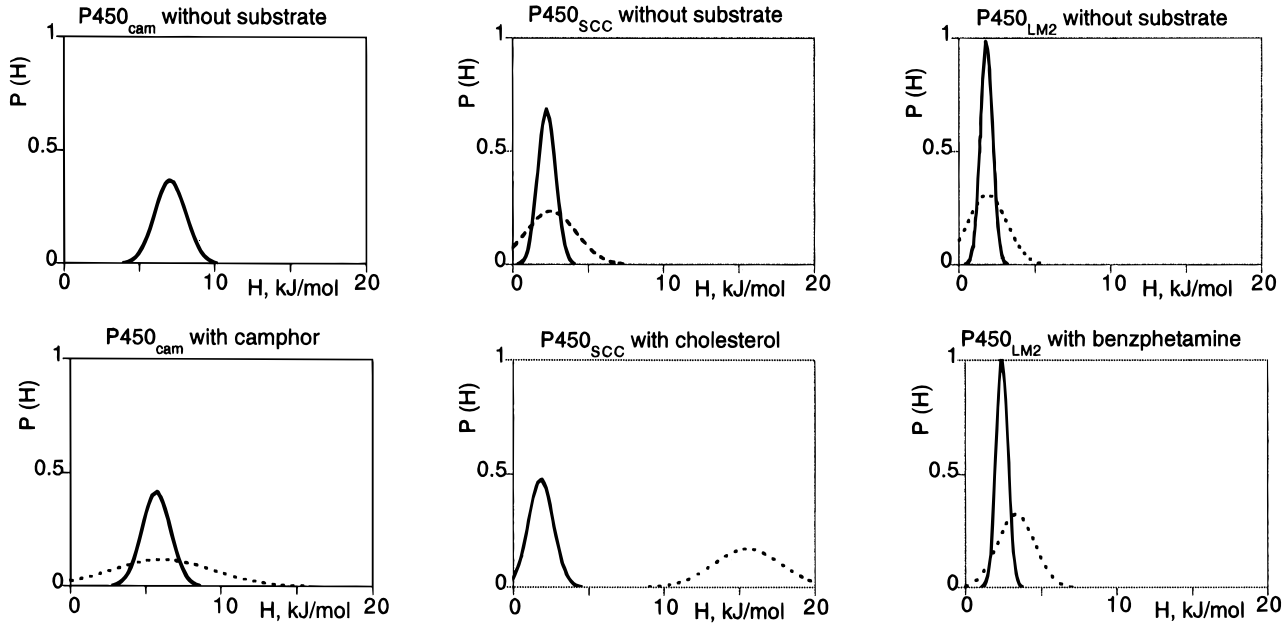

FIGURE 6: Normalized average enthalpy distributions $P(H,T_g)$ for each subdistribution. The average was computed by merging all $P(H)_T$ obtained below T_g and by applying a gaussian fit. Top: substrate-free forms of cytochromes P-450. Bottom: substrate-bound forms. Full and dotted lines correspond to the enthalpy distributions of the "fast" and "slow" sets of substates, respectively.

Table 2: Pre-Exponential Factors, Peak Enthalpies, and Enthalpy Widths Determined for the "Fast" and "Slow" Subpopulations Below T_g

molecule	log A_{fast} (s^{-1})	H_{fast} (kJ/mol)	width[a] (kJ/mol)	log $A_{slow,}$ (s^{-1})	H_{slow} (kJ/mol)	width[a] (kJ/mol)
$P450_{cam}$ m^{r}_{co}	9.6 (0.1)	7.3 (0.2)	2.4 (0.3)			
$P450_{cam}$ m^{rs}_{co}	8.9 (0.2)	5.7 (0.4)	2.2 (0.3)	7.3 (0.6)	6.1 (1.2)	7.9 (1.8)
$P450_{LM2}$ m^{r}_{co}	8.3 (0.1)	1.9 (0.2)	0.9 (0.1)	7.4 (0.1)	1.9 (0.5)	3.0 (0.4)
$P450_{LM2}$ m^{rs}_{co}	8.6 (0.1)	2.4 (0.2)	0.9 (0.1)	8.3 (0.2)	3.3 (0.3)	2.9 (0.2)
$P450_{scc}$ m^{r}_{co}	8.1 (0.1)	2.2 (0.1)	1.4 (0.1)	7.4 (0.2)	2.5 (0.4)	3.9 (0.5)
$P450_{scc}$ m^{rs}_{co}	7.7 (0.2)	1.8 (0.4)	2.0 (0.2)	9.9 (0.1)	15.5 (0.5)	5.3 (1.0)
Mb CO[b]	8.8	10.5	6.0			

[a] Full width at half maximum of the enthalpy distribution. [b] Data from Steinbach et al. (1992). Values in parentheses are standard deviations of the least square fit to eq 10.

DISCUSSION

1. Fluid Environment at Room Temperature. 1.1. Bimolecular Rate and Yield. Except for P-450_{LM2}, binding of the substrate causes the yield of the bimolecular process to increase up to $N_{esc} = 1.0$ and the bimolecular rate to decrease by 1 or 2 orders of magnitude. But even in the absence of a substrate, the yield of CO escape and the geminate and bimolecular rates differ markedly among cytochromes. Although we cannot extract the rate parameters unambiguously from the nonexponential geminate recombinations, k_{esc} and k_{int} must have comparable orders of magnitude in substrate-free forms ($0 < N_{esc} < 1$), whereas in presence of a bulky substrate $k_{esc} \gg k_{int}$ ($N_{esc} = 1$).

This means that ligand exit is facilitated but that its reentry becomes more difficult. The substrate may exert a dual effect upon the CO dynamics by interacting sterically with CO and/or by inducing conformational changes in the ligand access channel. Whereas steric effects in the vicinity of the heme can only decrease the internal binding rate and consequently increase N_{esc}, substrate-induced conformational changes can either hinder or facilitate diffusion of the ligand through the protein matrix by respectively restricting or enlarging the access channel. With most hemoproteins and heme models, internal rebinding has generally been found to be the rate-limiting step at room temperature (Doster et al., 1982; Tetreau et al., 1987). The bimolecular rate parameter k'_{on} can then be approximately factorized (Young, 1984) as

$$k'_{on} = k_{int}(k'_{ent}/k_{esc})N_{esc} \quad (14)$$

Hence, eqs 11, 12, and 14 indicate that a relative increase of k_{esc} and/or a relative decrease of k_{int} will lead both to the observed changes in N_{esc} and k_{on}. Due to the absence of geminate recombinations with substrate-bound P-450_{scc} and P-450_{cam}, the extent to which k_{int} is changed cannot be directly estimated. Extrapolation of low-temperature data (Discussion, section 2.4) tends to suggest that changes of k_{int} may not be sufficient to account for all of the observed effects and that an increase of k_{esc} is also likely to occur. Direct substrate−CO interaction is supported by the X-ray crystallographic data of P-450_{cam}: the Fe−C−O geometry is clearly distorted and the substrate is shifted by about 1 Å away from the heme upon CO binding (Raag & Poulos, 1989). The crystallographic structures of the Fe(III) substrate-free and substrate-bound forms provide no evidence of any important conformational change of the protein itself, except perhaps for a decrease in flexibility of some parts of the protein in the bound-form (Poulos et al., 1986; Poulos et al., 1987). Flexibility of the protein matrix is just what is required to affect k'_{ent} and k_{esc}. The structure of P-450_{scc} remains unknown. The present kinetic results indicate that cholesterol provides steric hindrance to CO binding with the

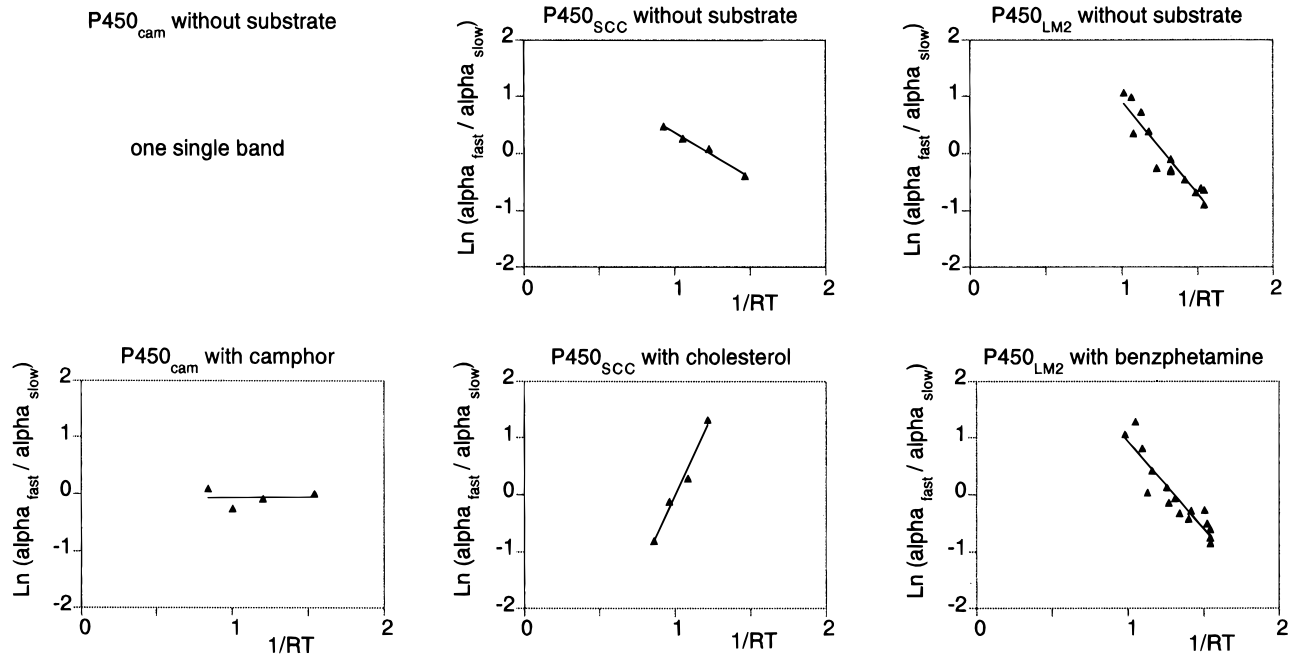

FIGURE 7: Relative populations a_{fast}/a_{slow} of the "fast" and "slow" reacting sets of CS for the substrate-free (top) and substrate-bound (bottom) forms of cytochromes P-450.

Table 3: Thermodynamic Parameters of the Equilibrium between the "Fast" and "Slow" Subpopulations of CS[a]

molecule	$\Delta S/R$	ΔH (kJ/mol)
P-450$_{cam}$ m$^{r}_{co}$		
P-450$_{cam}$ m$^{rs}_{co}$	−0.1 (0.4)	−0.0 (0.3)
P-450$_{LM2}$ m$^{r}_{co}$	4.2 (0.4)	3.2 (0.3)
P-450$_{LM2}$ m$^{rs}_{co}$	4.0 (0.4)	3.1 (0.3)
P-450$_{scc}$ m$^{r}_{co}$	1.9 (0.2)	1.6 (0.1)
P-450$_{scc}$ m$^{rs}_{co}$	−5.8 (0.6)	−5.8 (0.6)

[a] Values in parentheses are the standard deviations of the van't Hoff's plots (Figure 7).

heme, but that, in spite of the larger size of cholesterol compared to camphor, the effect is less pronounced than in the case of P-450$_{cam}$. This suggests that, in the presence of the substrate, the active site of P-450$_{scc}$ is not as tightly packed as that of P-450$_{cam}$. Finally, CO binding with the highly substrate-specific P-450$_{cam}$ and P-450$_{scc}$ is very sensitive to substrate binding.

In contrast, only minor changes are observed upon binding of benzphetamine with P-450$_{LM2}$. This highlights the particular flexibility of its active site which can accommodate substrates of various sizes and shapes, in accord with its poor substrate specificity. The effect of different polyaromatic hydrocarbons as substrates on the bimolecular CO binding with P-450$_{LM2}$ has been previously examined (Imai, 1982a; Imai, 1982b). Whereas hydrocarbons with a narrow, long, and flexible shape are relatively inefficient in reducing the rate of CO binding, those hydrocarbons having a bent and spreading structure are most effective in doing so. It was concluded that the substrate binding site is not rigid but rather shaped, in part, by the nature of the substrate. The relative internal mobility of benzphetamine could explain why it does not interfere with CO.

1.2. Nonexponential Geminate Process. One intriguing feature in Figure 2 is the nonexponential character of the geminate rebinding kinetics of the three cytochromes. Tian et al. (1995) observed that the geminate CO recombinations with P-450$_{cam}$ could be fitted to a sum of two exponentials. Our MEM rate spectrum confirms the presence of two relatively narrow peaks for P-450$_{cam}$ and P-450$_{LM2}$ while the P-450$_{scc}$ band is broad and unresolved. In our opinion, an interpretation of the kinetic heterogeneity in terms of protein conformers in slow exchange (Tian et al., 1995) is hazardous. The low temperature results, discussed in section 2.4, indicate that only one single geminate process is expected to be observed at room temperature. In addition, we observed that the initial absorbance changes are increased 2−3-fold when geminate recombinations become slower, and therefore more readily observable at low temperature. Presumably, the fast phase seen at room temperature is only a fraction of the whole geminate process which probably peaks around log $k = 8$. Whereas a truncation should be of no consequence for a purely exponential process, its effect on the fits to complex kinetics is unpredictable. We therefore believe that the apparent biphasic character of the geminate process is likely to be an artefact. Faster measurements are necessary in order to investigate the geminate process at room temperature more accurately.

1.3. Protein Relaxation. We suspect the nonexponential geminate phase at room temperature to be connected with the initial rise of absorbance shown in the rebinding kinetics of substrate-bound P-450$_{cam}$ and P-450$_{scc}$ (Figure 1). This signal was independent of the concentration of CO and, because of its small amplitude, could only be detected as a modulation occurring during the first few microseconds of the much slower bimolecular phase of substrate-bound P-450$_{cam}$ and P-450$_{scc}$ ($N_{esc} = 1.0$). A similar signal, if it were superimposed with the rapid geminate phase of all other P-450 complexes, would certainly remain hidden, but the geminate phase would appear nonexponential. The viscosity dependence argues in favor of a conformational change resulting in a time-dependent spectral shift of the photodissociated species as the initial photoproduct relaxes toward the ligand-free conformation. Other explanations, like spectral or kinetic hole burning (Campbell et al., 1987; Agmon, 1988; Ormos et al., 1990; Steinbach et al., 1991),

Scheme 2

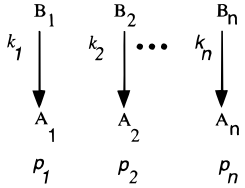

are also possible, but these effects are quite small in the Soret region where rebinding is monitored. Conformational relaxation is now well documented in myoglobin (Steinbach et al., 1991; Ansari et al., 1994). It occurs as a continuous process from picoseconds to about 10 μs in 70% glycerol (Jackson et al., 1994). The results of a recent photoacoustic calorimetry study of P-450$_{cam}$ suggest that, following photodissociation, the protein relaxes and that a salt bridge desolvates with a time constant of the order of 100 ns in pure buffer at 20 °C (Di Primo et al., 1997). Under similar conditions, we found the time constant of the initial absorbance rise to be about 500 ns when measured directly. These data prompt us to believe that conformational relaxation of cytochrome P-450 is at the origin of the nonexponential geminate kinetics at room temperature. A definite proof will evidently require considerably more detailed studies.

2. Rigid Environment and Low Temperatures. 2.1. Kinetic Connections among Substates. The distribution of activation enthalpies $P(H)$ shown in Figure 6, together with their temperature dependence (Figure 7) and pre-exponential factors are sufficient to explain all rebinding curves of cytochromes P-450 in a rigidified solvent below 165 K. In this section, we interpret the specific features of cytochromes P-450 in terms of kinetic connections between conformational substates. To avoid repetitions we first define two experimental time windows Θ_{kin} and Θ_{prep} which are implicit in all kinetic measurements but strongly condition the appearance of kinetic processes. Θ_{kin} is the total duration of the kinetic measurement starting with excitation and ending when the rebinding signal becomes negligible. Θ_{kin} was of the order of 1 s in our experiments. Θ_{prep} refers to the preparation time during which the sample is allowed to equilibrate following a temperature change. Θ_{prep} was of the order of 20 min.

Before the complex case of cytochromes P-450 is discussed, it is appropriate to summarize the basic hypotheses initially put forward for Mb by Frauenfelder and co-workers (Austin et al., 1975) and to outline their consequences which were thereafter confirmed with Hb chains (Doster et al., 1982; Dlott et al., 1983; Ansari et al., 1986), hemerythrin (Lavalette & Tetreau, 1988; Lavalette et al., 1991), and Azurin (Ehrenstein & Nienhaus, 1992).

(1) Proteins exist in a large number of conformational substates which rebind at different rates. Photodissociation brings the protein, initially in one of the bound substates (A_i), into the corresponding dissociated substate (B_i), from which subsequent rebinding takes place with rate k_i (Scheme 2).

(2) In a non-viscous solvent around 295 K, the rate of fluctuations between A_i as well as between B_i substates is higher than the rebinding rate. Under these conditions, the overall rebinding appears exponential. Its rate is the average value: $\langle k \rangle = \sum p_i k_i$, where p_i is the stationary probability of the B_i substate.

Scheme 3

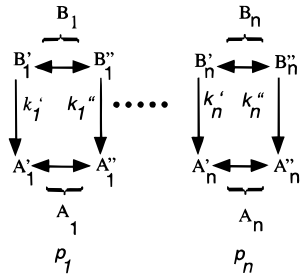

(3) In a rigid environment, e.g. at low temperature and high viscosity, rebinding is nonexponential because transitions among B_i substates do not take place and because each B_i substate decays to A_i independently on the time scale of the kinetic experiment ($k_{fluct} \ll 1/\Theta_{kin}$). The initial probability of each B_i substate equals that of the corresponding A_i substate from which it originates (assuming a uniform photodissociation efficiency). Transitions among A_i substates are also suppressed. The time required to thermally equilibrate A_i substates by far exceeds the experiment's preparation time ($k_{th} \ll 1/\Theta_{prep}$). The probabilities of A_i substates remain constant upon lowering the temperature below T_g. The enthalpy spectrum $P(H)_T = P(H,T_g) = P(H)$ is therefore invariant, though the rate spectrum continuously shifts as a consequence of the Arrhenius relationship.

In agreement with these considerations, the enthalpy distribution of P-450$_{cam}$ m^r_{co} consists of a single, temperature invariant, band which can be approximated by a gaussian.

The other forms of cytochromes P-450 exhibit new features which contrast with those reported earlier for different proteins: (*i*) measurements of CO rebinding performed in the Soret show that $P(H)$ is the sum of two subdistributions; (*ii*) each normalized subdistribution is temperature-invariant below T_g; (*iii*) the protein populations at the origin of the enthalpy subdistributions are in a dynamic, though very slow equilibrium well below T_g.

As a consequence, these data impose additional constraints to the kinetic scheme connecting A and B states. In particular, they imply two sets of B_i substates, a fast reacting set $\{F\} = \{B'_1, B'_2, ..., B'_n\}$ and a slow reacting set $\{S\} = \{B''_1, B''_2, ..., B''_n\}$. The nonexponential rebinding and the temperature invariance of each enthalpy subdistribution imply that the above "standard" hypotheses must be valid for each set individually. Substates within one set are thus kinetically and thermodynamically disconnected, i.e. transitions like $B'_i \leftrightarrow B'_j$ and $B''_p \leftrightarrow B''_q$ do not take place.

Yet both sets taken as a whole are in a thermodynamic equilibrium with each other below T_g, i.e. $\{F\} \leftrightarrow \{S\}$.

Because thermal equilibration could not propagate beyond the substates connecting {F} and {S} without violating the above constraint, the results exclude any sequential connection of these two distinct sets of substates. As a consequence, only parallel connections can exist between {S} and {F}. This leads to Scheme 3 which we interpret as follows. The $P(k)$ distributions are still caused by protein conformational substates A_i (bound CO) and B_i (photodissociated CO). These states are not connected below T_g. Therefore, they occur with constant probability p_i. The new feature is that conformational substates A_i and B_i exhibit a fine structure and split into two primed states with contrasted kinetic properties (e.g. $k'_i \gg k''_i$). As indicated thermal equilibration is allowed among primed substates within each A_i or B_i state.

In this model, $B'_i \rightarrow A'_i$ and $B''_i \rightarrow A''_i$ transitions take place with activation enthalpies H'_i and H''_i and pre-exponentials log A' and log A'' which respectively give rise to the fast and slow distribution.

Scheme 3 is the most general one consistent with the kinetics of cytochromes P-450 but the data give further indications about the order of magnitude of the relaxation rates between primed substates.

Consider first one particular B_i state and the equilibrium $B'_i \leftrightarrow B''_i$. If this equilibrium was to relax faster than the rebinding, the fast and slow rates would combine into an average rate: $\langle k_i \rangle = \alpha_i k_{fast} + \beta_i k_{slow}$ where α_i and β_i are the fractional occupations. Thus $\langle k_i \rangle$ would change somewhat with temperature keeping the total probability $p_i = \alpha_i + \beta_i$ constant. This case only predicts a stretch or a compression of the domain of rate parameters, without affecting the overall profile of the probability distribution. It cannot account for two independent $P(H)$ bands. The data thus exclude the possibility of thermal equilibration between B_i substates being faster than rebinding. Exchange between photodissociated B_i substates has been observed by others, but only on a much longer time scale. At 40 K, rebinding of photodissociated P-450$_{cam}$ is so slow that IR spectra of the trapped dissociated species can be recorded using a conventional FTIR spectrometer. After the temperature was raised to 100 K, a second record showed distinct changes of the IR spectrum, proving that at least some amount of re-equilibration had been taking place (Jung et al., 1992). There is however no contradiction with the present conclusions since these experiments were performed on a time scale of several minutes.

Primed A_i states are spectroscopically and kinetically undistinguishable under observation in the Soret. Analogy with B_i states suggests that thermal equilibration $A'_i \leftrightarrow A''_i$ could be slow. But whereas the overall rebinding kinetics probes the B_i states for a maximum of $\Theta_{kin} = 1$ s, the equilibrium $A'_i \leftrightarrow A''_i$ may relax over a period as long as $\Theta_{prep} = 30$ min. In contrast, the barrier between A_1, A_2, A_3, ... (due both to temperature and to the rigidity of the solvent) cannot be overcome and thermal equilibration between these states is never achieved. Since re-equilibration among A'_i and A''_i states does not affect the total probability p_i of substate A_i, the result of its splitting is to give rise to the superposition of two distinct enthalpy distributions: $\{H_{fast}\} = \{\ln A'; H'_i; \alpha_i p_i\}$ and $\{H_{slow}\} = \{\ln A''; H''_i; \beta_i p_i\}$. They may differ in H_{peak} and pre-exponential factor. Their relative weight is expected to vary according to

$$\alpha/\beta = \sum \alpha_i p_i / \sum \beta_i p_i \qquad (15)$$

In general the temperature dependence will not be a simple exponential unless the ratio α_i/β_i is identical in all pairs of primed states. Because CS are structurally close to each other, it is reasonable to speculate that the (unknown) structural perturbation which is at the origin of the splitting of the CS induces a constant free energy difference between the wells of $A'_i - A''_i$ pairs. Despite some scatter and the limited temperature range (77 to about 125 K), the data are not inconsistent with an exponential (Figure 7).

Therefore the extended Scheme 3 accounts for the main features of the bimodal $P(H)$ in cytochromes P-450.

2.2. Hierarchy of Substates: Differences with Mb. Spectroscopic and kinetic studies of Mb (Ansari et al., 1985,-1987; Berendzen & Braunstein 1990; Mourant et al., 1993; Johnson et al., 1996) have revealed that conformational substates are organized in a hierarchy of several tiers arranged by decreasing barrier heights. The series of conformational substates are respectively denoted CS^0, CS^1, CS^2, etc. In this section, we examine how this model must be adapted to fit the kinetic scheme of cytochromes P-450.

(a) CS^0 Substates. The CS^0 substates of Mb have been named "taxonomic macroscopic" substates, because they are characterized by different resolvable infrared stretch bands of the bound CO. These bands are thought to differ essentially in the Fe−C−O angle (Kuriyan et al., 1986; Ormos et al., 1988; Cheng et al., 1991) or in the dipolar interactions of the ligand with different distal environments (Li et al., 1994; Johnson et al., 1996). Monitoring the kinetics of CO rebinding in the infrared CO stretch bands showed that different CS^0 rebind with distinct kinetics and that each CS^0 consists of a large number of particular CS^1. Thus, each CS^0 is characterized by a distinct $P(H)$. In the visible (Soret) region only the average $P(H)$ can be observed because the spectral features are dominated by the heme group and because CS^0 substates are not resolved spectroscopically (Ansari et al., 1987).

Even though our present knowledge on structure and spectroscopic markers of cytochromes P-450 is quite incomplete, it seems very likely that CS^0 substates, characterized by their different distal environment or geometry of the Fe−CO bond, also exist in cytochromes P-450. The infrared spectra of cytochrome P-450$_{cam}$ in its Fe(II)−CO bound state indicate the presence of multiple CO stretching bands. The substrate-free and substrate-bound forms respectively present 6 or 2 different bands which, like in Mb, do not interconvert below about 180 K (Jung & Marlow, 1987; Jung et al., 1992, 1996). Infrared spectra at low temperatures are not yet available for P-450$_{LM2}$ and P-450$_{scc}$. While, at room temperature, one relatively sharp infrared band was detected with P-450$_{scc}$ m^r_{co} and m^{rs}_{co} (Tsubaki et al., 1992), one broad band was observed for P-450$_{LM2}$ m^r_{co} (O'Keefe et al., 1978). No data are yet available for the substrate-bound form of P-450$_{LM2}$. Since the present work was performed by monitoring in the Soret, the kinetics are representative of the average rebinding to all CS^0 substates considered as a whole. CS^0 substates cannot be responsible for the bimodal enthalpy distributions, in agreement with the kinetic discussion of section 2.1.

(b) CS^1 Substates. Evidence for CS^1 substates comes from the nonexponential rebinding at low temperature and from the resulting enthalpy spectrum both of which show that rebinding occurs from a large number of substates. But the temperature dependence of the bimodal enthalpy distribution of cytochromes P-450 has no equivalent in Mb. In Mb, each CS^1 substate is a "singlet", characterized by one unique activation enthalpy. The presence of substates of the lower tier, CS^2, which may still equilibrate even below 77 K, accounts for the "line width". The enthalpy spectrum is the envelope of the contributions of all CS^1 substates.

The particular kinetic connections of substates in cytochromes P-450 (section 2.1) imply that, at about 100 K, CS^0 do not equilibrate and that CS^1 substates appear in fact as "doublets" ($CS'^1-CS''^1$) separated by a free energy barrier intermediate between the barrier separating CS^1 and that separating CS^2 substates. Experiments indicate that the time required to equilibrate primed CS^1 substates following a

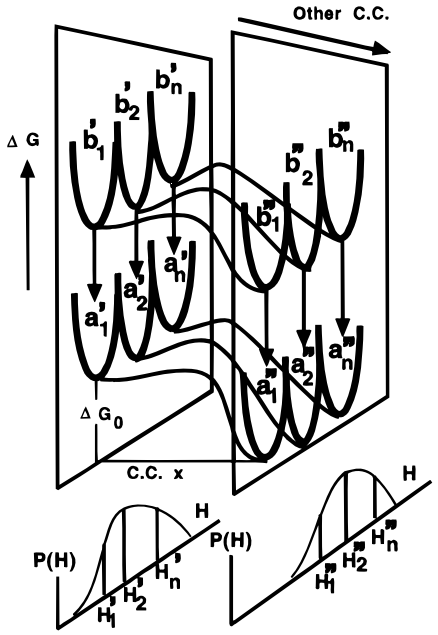

FIGURE 8: Sketch of the free-energy diagram of cytochromes P-450. Each plane represents a section through the free-energy surface along all conformational coordinates except one, labeled "x". CS^1 substates, shown in heavy lines, are totally isolated by large energy barriers due to the rigid environment. The reaction coordinate along which photodissociation and rebinding occur cannot be represented in this 3D diagram. It is suggested by vertical arrows connecting dissociated "b" substates with liganded "a" substates and by distinct activation enthalpy distributions $P(H)$ at the bottom of each plane. Conformational coordinate "x" connects the components of doublet CS^1 via energy barriers which can be overcome during the preparation time Θ_{prep}. Presumably, conformational coordinate "x" is an internal one, corresponding to groups of atoms which have no direct interaction with the solvent and may keep some residual, though constrained, degrees of freedom. Because doublet pairs do not have time to equilibrate during rebinding, two distinct $P(H)$ are observed. However thermal equilibration along coordinate "x" does occur during Θ_{prep}, and the ratio of the two distributions is temperature dependent. In this diagram we made the simplifying assumption that CS^1 substates in one plane are uniformly shifted by a constant amount ΔG_0 compared to the CS^1 of the other plane. Fine structure due to CS^2 substates has been omitted for clarity. In myoglobin or isolated hemoglobin chains, only one plane and one $P(H)$ is sufficient to account for the rebinding dynamics.

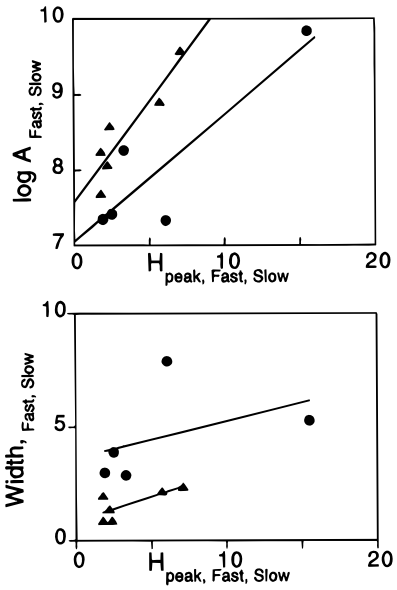

FIGURE 9: Top: entropy−enthalpy correlations. Bottom: correlation between the width of $P(H)$ and its peak enthalpy value. Triangles and circles are for the "fast" and "slow" subdistributions, respectively.

temperature change must be in the range of seconds to a few minutes. The free energy barrier between the doublets is thus of the order of 20−30 kJ/mol at 100 K. The arrangement of the CS^1 substates in cytochromes P-450 is sketched in Figure 8.

The equilibrium ΔH and $\Delta S/R$ values reported in Table 3 were based on the logarithm of the $\alpha_{fast}/\alpha_{slow}$ ratio, and some values are of opposite sign. A more regular pattern is obtained by considering the doublet component which dominates at high temperature, irrespective of its kinetic character. With this convention, the doublet component which dominates at room temperature has, by definition, the higher enthalpy. It happens also to have the higher entropy. Figure 9 illustrates this entropy−enthalpy correlation.

(c) Substates Hierarchy and Barrier Height. The classification of substates according to free energy barrier height may sometimes be an ambiguous concept when dealing with proteins. Because cryoprotective cosolvents are needed to explore a wide temperature range, protein motions are submitted to large changes in the ambient viscosity. It has been shown, namely through observations of nonexponential kinetics, even at room temperature, in a rigid or very viscous environment (Austin et al., 1975; Lavalette & Tetreau, 1988; Hagen et al., 1995), that the solvent's temperature-dependent viscosity controls most of the apparent free energy barrier. Not only does viscous damping depend on the motions's frequency but it is also expected to differently affect the groups of residues which are exposed to the solvent as well as those which are buried deeply within the protein. Thus a free-energy diagram, such as the one shown in Figure 8, should rather be considered as an empirical sketch of those motions which may be observed within the time windows Θ_{kin} and Θ_{prep} under particular experimental conditions of temperature and viscosity.

2.3. Thermodynamic Characteristics of the Subdistributions. The peak activation enthalpies, bandwidths, and pre-exponential factors of the cytochrome P-450−CO complexes are systematically and significantly less than corresponding values of myoglobin (Table 2). The pre-exponential factors are positively correlated with H_{peak}, but "slow" and "fast" distributions follow distinct correlations (Figure 9, top). The $P(H)$ band which corresponds to the fastest component of the kinetics is narrow (bandwidth between 0.9 and 2.5 kJ/mol, while the slow $P(H)$ band is much broader (3−8 kJ/mol). The width of $P(H)$ also tends to increase slowly with H_{peak}, but the "slow" distributions tend to be broader (Figure 9, bottom).

Globally, the components of the CS'^1−CS''^1 doublets display very different properties, a case that may be qualified as strong symmetry breaking (Ansari et al., 1987). This is rather fortunate, since without the difference in log A, the resolution of $P(H)$ into two bands would hardly have been possible.

2.4. Substrate Binding and Connection with Room Temperature Data. Substrate binding was found to exert a profound effect on the CO binding with P-450_{cam} and P-450_{scc} at room temperature. At low temperature, the effect is remarkable as well: the number of bands in $P(H)$ is changed from 1 to 2 in P-450_{cam}, and the two bands of P-450_{scc} undergo significant changes. Apparently, P-450_{LM2} is only

Table 4: Average Internal Rebinding Rate at $T_g = 165$ K Extrapolated Using $P(H)$ and log A

molecule	$\langle k_{int} \rangle$ (10^8 s^{-1})	molecule	$\langle k_{int} \rangle$ (10^8 s^{-1})
P-450$_{cam}$ m$^{r}_{co}$	6.5	P-450$_{LM2}$ m$^{rs}_{co}$	2.0
P-450$_{cam}$ m$^{rs}_{co}$	1.6	P-450$_{scc}$ m$^{r}_{co}$	0.4
P-450$_{LM2}$ m$^{r}_{co}$	0.9	P-450$_{scc}$ m$^{rs}_{co}$	1.4

marginally sensitive to substrate binding both at room and low temperature.

Extrapolation of the equilibrium of the CS′−CS″ subpopulations indicates that the dominant species at room temperature should be "fast", except for substrate-bound P-450$_{scc}$. Since $P(H)$ profiles are constant below $T_g = 165$ K, an average rebinding rate $\langle k_{int} \rangle$ can be computed for any temperature up to T_g. For this particular temperature, $P(H) = P(H,T_g)$ is then an equilibrium distribution and thus $\langle k_{int} \rangle$ corresponds to the rate that would be observed if fast equilibrium fluctuations were restored and rebinding were exponential, i.e. $k_{int} = (\langle k_{fast} \rangle$ or $\langle k_{slow} \rangle)$. Extrapolation above 165 K is not legitimate, because we do not know how $P(H,T)$ behaves above T_g. The data shown in Table 4 indicate that, even at such a low temperature, $\langle k_{int} \rangle$ is of the order of 1×10^8 s^{-1} and that the changes induced by substrate binding are less than 3-fold. Of course, low-temperature data do not give information about k_{esc}. However, in order to account for the decrease of the bimolecular rebinding rate as well as for the increased value of N_{esc} (section 1.1), the relatively modest changes expected for $\langle k_{int} \rangle$ support the view that significant changes in k_{esc} must take place at higher temperatures.

2.5. Origin and Properties of the Doublet Substates. There are evidently some basic differences between the active site of oxygen carrier hemoproteins and that of cytochromes P-450. The first is the ability of cytochromes to bind a substrate. Although the kinetic properties of the doublets are quite sensitive to substrate binding, the fact that even substrate-free P-450$_{LM2}$ and P-450$_{scc}$ present subdistributions rules out the substrate as a cause of the existence of doublet substates in cytochromes P-450. We do not know whether substrate-free P-450$_{cam}$ is an exception, with only singlet substates, or whether its doublet substates are not kinetically distinguishable.

The cause for the existence of doublet substates must be found elsewhere. Whereas most, if not all, features of the substates hierarchy in Mb have been explained by invoking the distal environment of the heme only, we suggest that proximal effects should be investigated as the possible origin of the different substates hierarchy in cytochromes P-450 because (i) a structural perturbation of the heme's proximal coordinate would probably affect all CS^1 substates to a similar extent and (ii) as the thiolate side chain is buried within the protein matrix, its motions may be only moderately damped by viscosity. A study comparing the local dynamics of the protein chains involved in the proximal heme side would certainly be of great value. Since only small atomic displacements subsist at temperatures below the freezing point of the solvent, the doublet CS^1 substates can differ only by the displacement of very few atoms, the overall protein structure remaining identical. In view of the present lack of structural data on P-450$_{scc}$ and P-450$_{LM2}$, testing this hypothesis raises a challenge to molecular modeling, especially as additional distal−proximal interactions may be required in order to account for the kinetic properties of the doublet substates.

SUMMARY OF CONCLUSIONS

Following photodissociation of carbonylated cytochromes P-450 in a fluid solvent at room temperature, both geminate recombinations and bimolecular rebinding are observed. Whereas the latter process is essentially exponential, geminate rebinding is rendered complex and nonexponential, presumably because of a spectral shift induced by protein relaxation on the same time scale. Binding of a substrate to cytochromes P-450$_{cam}$ and P-450$_{scc}$ causes the yield of the bimolecular process to increase up to $N_{esc} = 1.0$ and the bimolecular rate to decrease by 1 or 2 orders of magnitude. In contrast, only minor changes are observed upon binding of benzphetamine to P-450$_{LM2}$. The effect may therefore be correlated with substrate specificity.

As is the case with other proteins, conformational substates (CS^1) of cytochromes P-450 are at the origin of a distribution $P(k)$ of the geminate rate in a rigid environment at low temperature. However, in contrast with myoglobin, the enthalpy distribution $P(H)$ generally consists of a sum of two distinct subdistributions even in the absence of a substrate. Still more surprising is the fact that the subdistributions remain thermally equilibrated down to 77 K. We explain these findings by a splitting of each CS^1 into a pair of "doublet states" with contrasted dynamic properties. These doublet states are separated by energy barriers which are intermediate between those of CS^1 and CS^2 conformational substates, thus introducing additional complexity in the hierarchy of the conformational substates of hemoproteins. Though the structural fluctuations responsible for the splitting are not yet known, some arguments tend to favor explanations involving the proximal thiolate ligand.

ACKNOWLEDGMENT

We are greatly indebted to Dr. J.-C. Brochon for the adaptation of the MEM program to flash photolysis experiments. Thanks are due to J.-M. Lentz for expert assistance in developing the laser flash photolysis system. We thank the University of Illinois, Urbana, and Professor S. Sligar for the generous gift of the cytochrome P-450$_{cam}$ strain. We are grateful to Dr. Hui Bon Hoa for stimulating discussions during the elaboration phase of this work and to Dr. Vincent Ponette for proofreading the manuscript.

REFERENCES

Agmon, N. (1988) *Biochemistry 27*, 3507−3511.
Ansari, A., Berendzen, J., Bowne, S. F., Frauenfelder, H., Iben, I. E. T., Sauke, T. B., Shyamsunder, E., & Young, R. D. (1985) *Proc. Natl. Acad. Sci. U.S.A. 82*, 5000−5004.
Ansari, A., DiIorio, E. E., Dlott, D. D., Frauenfelder, H., Iben, I. E. T., Langer, P., Roder, H., Sauke, T. B., & Shyamsunder, E. (1986) *Biochemistry 25*, 3139−3146.
Ansari, A., Berendzen, J., Braunstein, D., Cowen, B. R., Frauenfelder, H., Hong, M. K., Iben, I. E. T., Johnson, J. B., Ormos, P., Sauke, T. B., Scholl, R., Schulte, A., Steinbach, P. J., Vittitow, J., & Young, R. D. (1987) *Biophys. Chem. 26*, 337−355.
Ansari, A., Jones, C. M., Henry, E. R., Hofrichter, J., & Eaton, W. A. (1994) *Biochemistry 33*, 5128−5145.
Austin, R. H., Beeson, K. W., Eisenstein, L., Frauenfelder, H., & Gunsalus, I. C. (1975) *Biochemistry 14*, 5355−5373.
Austin, R. H., Beeson, K. W., Chan, S. S., Debrunner, P. G., Downing, R., Eisenstein, L., Frauenfelder, H., & Nordlund, T. M. (1976) *Rev. Sci. Instrum. 47*, 445−447.

Berendzen, J., & Braunstein, D. (1990) *Proc. Natl. Acad. Sci. U.S.A. 87*, 1−5.
Campbell, B. F., Chance, M. R., & Friedman, J. M. (1987) *Science 238*, 373−376.
Cheng, X., & Scoenborn, B. P. (1991) *J. Mol. Biol. 220*, 381−399.
Di Primo, C., Deprez, E., Sligar, S. G., & Hui Bon Hoa, G. (1997) *Biochemistry 36*, 112−118.
Dlott, D. D., Frauenfelder, H., Langer, P., Roder, H., & DiIorio, E. E. (1983) *Proc. Natl. Acad. Sci. U.S.A. 80*, 6239−6243.
Doster, W., Beece, D., Bowne, S. F., DiIorio, E. E., Eisenstein, L., Frauenfelder, H., Reinisch, L., Shymsunder, E., Winterhalter, K. H., & Yue, K. T. (1982) *Biochemistry 21*, 4831−4839.
Ehrenstein, D., & Nienhaus, G. U. (1992) *Proc. Natl. Acad. Sci. U.S.A. 89*, 9681−9685.
Eisenstein, L. (1977) *Int. J. Quantum Chem. 4*, 363−374.
Gray, R. D. (1982) *J. Biol. Chem. 257*, 1086−1094.
Hagen, S. J., Hofrichter, J., & Eaton, W. A. (1995) *Science 269*, 959−962.
Hildebrandt, P., Heibel, G., Anzenbacher, P., Lange, R., Krüger, V., & Stier, A. (1994) *Biochemistry 33*, 12920−9.
Imai, Y. (1982a) *J. Biochem. 92*, 67−75.
Imai, Y. (1982b) *J. Biochem. 92*, 778−88.
Imai, Y., Hashimoto-Yutsodo, C., Satake, H., Girardin, A., & Sato, R. (1980) *J. Biochem. (Tokyo) 88*, 489−503.
Jackson, T. A., Lim, M., & Anfinrud, P. A. (1994) *Chem. Phys. 180*, 131−140.
Johnson, J. B., Lamb, D. C., Frauenfelder, H., Müller, J., McMahon, B., Nienhaus, G. U., & Young, R. D. (1996) *Biophys. J. 71*, 1563−1573.
Jung, C., & Marlow, F. (1987) *Stud. Biophys. 120*, 241−251.
Jung, C., Scholl, R., Frauenfelder, H., & Hui Bon Hoa, G. (1992a) in *Cytochromes P-450: Biochemistry and Biophysics* (Archakov, A. I., & Bachmanova, G. I., Eds) INCO-TNC, Joint Stock Company, Moscow.
Jung, C., Hui Bon Hoa, G., Schröder, K.-L., Simon, M., & Doucet, J.-P. (1992b) *Biochemistry 31*, 12855−12862.
Jung, C., Ristau, O., Schulze, H., & Sligar, S. G. (1996) *Eur. Biochem. J.* 235, 660−669.
Kashem, M. A., Lambeir, A.-M., & Dunford, H. B. (1987) *Biochim. Biophys. Acta 911*, 162−167.
Kuriyan, J., Wilz, S., Karplus, M., & Petsko, G. A. (1986) *J. Mol. Biol. 192*, 133−154.
Lange, R., Maurin, L., Larroque, C., & Bienvenue, A. (1988) *Eur. J. Biochem. 172*, 189−195.
Lange, R., Larroque, C., & Anzenbacher, P. (1992a) *Eur. J. Biochem. 207*, 69−73.
Lange, R., Pantaloni, A., & Saldana, J.-L. (1992b) *Eur. J. Biochem. 207*, 75−79.
Lange, R., Heiber-Langer, I., Bonfils, C., Fabre, I., Negishi, M., & Balny, C. (1994) *Biophys. J. 66*, 89−98.
Larroque, C., & Van Lier, J. E. (1986) *J. Biol. Chem. 261*, 1083−1087.
Lavalette, D., & Tetreau, C. (1988) *Eur. J. Biochem. 177*, 97−108.
Lavalette, D., Tetreau, C., Brochon, J.-C., & Livesey, A. (1991) *Eur. J. Biochem. 196*, 591−598.
Li, T., Quillin, M. L., Phillips Jr, G. N., & Olson, J. S. (1994) *Biochemistry 33*, 1433−1446.
Lim, M., K, Jackson, T. A., & Anfinrud, P. A. (1993) *Proc. Natl. Acad. Sci. U.S.A. 90*, 5801−5804.
Livesey, A. K., & Brochon, J.-C. (1987) *Biophys. J. 52*, 693−706.
Livesey, A. K., Delaye, M., Licinio, P., & Brochon, J.-C. (1987) *Faraday Disc. Chem. Soc. 83*, 1−12.
Mitani, F., Iizuka, T., Shimada, H., Ueno, R., & Ishimura, Y. (1985) *J. Biol. Chem. 260*, 12042−12048.
Mourant, J. R., Braunstein, D. P., Chu, K., Fauenfelder, Hans, Nienhaus, G. U., Ormos, P., & Young, R. D. (1993) *Biophys. J. 65*, 1496−1507.
Nienhaus, G. U., Mourant, J. R., & Frauenfelder, H. (1992) *Proc. Natl. Acad. Sci. U.S.A. 89*, 2902−2906.
Oertle, M., Richter, C., Winterhalter, K. H., & DI Iorio, E. E. (1985) *Proc. Natl. Acad. Sci. USA 82*, 4900−4904.
O'Keefe, D. H., Ebel, R. E., Peterson, J. A., Maxwell, J. C., & Caughey, W. S. (1978) *Biochemistry 17*, 5845−5852.
Ormos, P., Brauenstein, D., Frauenfelder, H., Hong, M. K., Lin, S.-L., Sauke, T. S., & Young, R. D. (1988) *Proc. Natl. Acad. Sci. U.S.A. 85*, 8492−8496.
Ormos, P., Ansari, A., Braunstein, D., Cowen, B. R., Frauenfelder, H., Hong, M. K., Iben, I. E. T., Sauke, T. B., Steinbach, P. J., & Young, R. D. (1990) *Biophys. J. 57*, 191−199.
Poulos, T. L., Finzel, B. C., & Howard, A. J. (1986) *Biochemistry 25*, 5314−5322.
Poulos, T. L., Finzel, B. C., & Howard, A. J. (1987) *J. Mol. Biol. 195*, 687−700.
Raag, R., & Poulos, T. L. (1989) *Biochemistry 28*, 7586−7592.
Steinbach, P. J. (1996) *Biophys. J. 70*, 1521−1528.
Steinbach, P. J., Ansari, A., Berendzen, J., Braunstein, D., Chu, K., Cowen, B. R., Ehrenstein, D., Frauenfelder, H., Bruce Johnson, J., Lamb, D. C., Luck, S., Mourant, J. R., Nienhaus, G. U., Ormos, P., Philipp, R., Xie, A., & Young, R. D. (1991) *Biochemistry 30*, 3988−4001.
Steinbach, P. J., Chu, K., Frauenfelder, H., Johnson, J. B., Lamb, D. C., Nienhaus, G. U., Sauke, T. B., & Young, R. D. (1992) *Biophys. J. 61*, 235−245.
Suhara, K., Gomi, T., Sato, H., Itagaki, E., Takemori, S., & Katagiri, M. (1978) *Arch. Biochem. Biophys. 190*, 290−299.
Tetreau, C., Lavalette, D., Momenteau, M., & Lhoste, J.-M. (1987) *Proc. Natl. Acad. Sci. U.S.A. 84*, 2267−2271.
Tian, W. D., Wells, A. V., Champion, P. M., Di Primo, C., Gerber, N., & Sligar, S. G. (1995) *J. Biol. Chem. 270*, 8673−8679.
Tsubaki, M., Yoshikawa, S., Ichikawa, Y., & Yu, N.-T. (1992) *Biochemistry 31*, 8991−8999.
Tuckey, R. C., & Kamin, H. (1983) *J. Biol. Chem. 258*, 4232−4237.
Unger, B. P., Gunsalus, I. C., & Sligar, S. G.. (1986) *J. Biol. Chem. 261*, 1158−1163.
Young, R. D. (1984) *J. Chem. Phys. 80*, 554−560.

BI970619M